Available online at www.sciencedirect.com
SCIENCE DIRECT®
Journal of Solid State Chemistry 177 (2004) 3633–3639
JOURNAL OF SOLID STATE CHEMISTRY
http://elsevier.com/locate/jssc

# Magnetic properties of $La_{0.5-x}Ln_xSr_{0.5}MnO_3$ ($Ln$ = Pr, Nd, Gd and Y)

Md. Motin Seikh,[a,b] L. Sudheendra,[b] and C.N.R. Rao[a,b,*]

[a] *Solid State and Structural Chemistry Unit, Indian Institute of Science, Bangalore-560 012, India*
[b] *Chemistry and Physics of Materials Unit, Jawaharlal Nehru Centre for Advanced Scientific Research, Jakkur P.O., Bangalore-560 064, India*

Received 24 March 2004; received in revised form 14 May 2004; accepted 2 June 2004

Available online 19 August 2004

**Abstract**

Magnetic and electron transport properties of four series of manganates of the composition $La_{0.5-x}Ln_xSr_{0.5}MnO_3$ ($Ln$ = Pr, Nd, Gd and Y) have been investigated to examine how the ferromagnetic metallic nature of the parent La compound changes over to antiferromagnetic insulating behavior, with change in $Ln$ and $x$ due to the associated changes in the A-site cation radius as well as the size disorder. When $Ln$ = Pr and Nd, there is a transition from the tetragonal $I4/mcm$ structure to the orthorhombic *Immm* and *Imma* structures at $x = 0.2$ and 0.35, respectively. There is a gradual evolution of the properties from those of $La_{0.5}Sr_{0.5}MnO_3$ to those of $Pr_{0.5}Sr_{0.5}MnO_3$ or $Nd_{0.5}Sr_{0.5}MnO_3$ with increase in $x$. Thus, when $x > 0.2$ and $> 0.35$, respectively, the Pr- and Nd-substituted manganates show ferromagnetic transitions followed by antiferromagnetic transitions at low temperatures, with the ferromagnetic $T_C$ decreasing with increasing $x$. The Gd and Y series of compounds are all orthorhombic and show a decrease in $T_C$ with the increase in $x$, the ferromagnetism disappearing at high $x$. At a value of $x$ corresponding to the A-site cation radius of $Pr_{0.5}Sr_{0.5}MnO_3$, the Gd and Y series of compounds exhibit ferromagnetism in the 250–300 K region and undergo an antiferromagnetic transition on cooling. The $T_C - T_N$ gap is sensitive to the disorder arising from the size mismatch.


*Keywords:* Manganates, rare earth; Ferromagnetism, in rare earth manganates; Jahn–Teller distortion; Size-disorder, in rare earth manganates

## 1. Introduction

Several rare earth manganates of the general formula $Ln_{1-x}A_xMnO_3$ ($Ln$ = La and $A$ = Sr) exhibit ferromagnetism and metallicity [1]. Accordingly, $La_{0.5}Sr_{0.5}MnO_3$ ($I4/mcm$), with an average $A$-site cation radius, $\langle r_A \rangle$ of 1.263 Å is metallic and ferromagnetic at room temperature [2]. On the other hand, $Nd_{0.5}Sr_{0.5}MnO_3$ (*Imma*) with an $\langle r_A \rangle$ of 1.236 Å is metallic and ferromagnetic just below room temperature and becomes an antiferromagnetic (CE-type) charge-ordered insulator around 150 K [3–5]. $Pr_{0.5}Sr_{0.5}MnO_3$ with an $\langle r_A \rangle$ of 1.245 Å is also ferromagnetic below room temperature ($T_C = \sim 260$ K) and becomes anitferromagnetic ($A$-type) at $T_N = \sim 150$ K, but without charge ordering [4,5]. $Gd_{0.5}Sr_{0.5}MnO_3$ ($\langle r_A \rangle = 1.209$ Å) crystallizes in the *Pbnm* space group but does not show a distinct ferromagnetism, instead exhibiting a spin glass or cluster glass-type behavior at low temperatures [6,7]. The main causes for the drastic changes in the magnetic and electron transport properties of $Ln_{0.5}Sr_{0.5}MnO_3$ ($Ln$ = La, Pr, Nd or Gd) with $Ln$ is the change in $\langle r_A \rangle$ and the size disorder, $\sigma^2$, defined as $\sigma^2 = \sum x_i r_i^2 - (\langle r_A \rangle)^2$, where $x_i$ is the fractional occupancy of the $A$-site and $r_i$ is the corresponding ionic radii [8–10]. The metal–insulator transition, which can be induced as a function of $\langle r_A \rangle$ at constant doping, is generally accompanied by significant structural changes [11,12]. Thus, the Mn–O–Mn bond angle is a critical factor in determining the nature of magnetic transitions in manganates. Among the possible causes of carrier localization in the manganates, two of the important ones are the Jahn–Teller distortion and the change in $\langle r_A \rangle$ [8–15]. The local lattice distortion plays a crucial role in determining the properties of the doped manganates [16].

*Corresponding author. Chemistry and Physics of Materials Unit, Jawaharlal Nehru Centre for Advanced Scientific Research, Jakkur P.O., Bangalore-560 064, India. Fax: +91-80-2362-2766.
*E-mail address:* cnrrao@jncasr.ac.in (C.N.R. Rao).

0022-4596/$ - see front matter © 2004 Elsevier Inc. All rights reserved.
doi:10.1016/j.jssc.2004.06.004

Although several studies of $Ln_{0.5}Sr_{0.5}MnO_3$ with different rare earths have been reported in the literature [1–4,6,7,17–23], we considered it necessary to investigate the $La_{0.5-x}Ln_xSr_{0.5}MnO_3$ system with $Ln$ = Pr, Nd, Gd and Y to understand how the structure as well as the magnetic and electron transport properties change through the series due to the accompanying changes in $\langle r_A \rangle$ and related factors. In particular, it was of interest to examine how the ferromagnetism and metallicity of the parent manganate ($x = 0.0$) changes over to give rise to antiferromagnetism and insulating behavior at low temperatures. In $La_{0.5-x}Pr_x(Nd_x)Sr_{0.5}MnO_3$, an aspect that we have explored was to find out whether the properties of $Pr_{0.5}Sr_{0.5}MnO_3$ and $Nd_{0.5}Sr_{0.5}MnO_3$ manifest themselves at some composition. Equally important was our intention to study how the properties of $La_{0.5-x}Ln_xSr_{0.5}MnO_3$ ($Ln$ = Gd and Y) change when the $\langle r_A \rangle$ is close to that of the $Nd_{0.5}Sr_{0.5}MnO_3$ or $Pr_{0.5}Sr_{0.5}MnO_3$, the nature of antiferromagnetic ordering at low temperature being of specific interest. The relative sensitivities of $T_C$ and $T_N$ or the $T_C - T_N$ gap to structural factors and size disorder in these manganate compositions was another aspect of interest. It is to be noted that in the system under study, the carrier concentration is fixed. Hence, the changes in the structural features and local distortions brought about by the changes in $\langle r_A \rangle$ and the associated disorder are primarily responsible for affecting the magnetic and transport properties.

## 2. Experimental details

Polycrystalline samples of $La_{0.5-x}Ln_xSr_{0.5}MnO_3$ ($Ln$ = Pr, Nd, Gd and Y) were prepared by the reaction of stoichiometric amounts of the $Ln$(acetate), $SrCO_3$ and $MnO_2$ in the solid state. The initial mixture was ground thoroughly in an agate mortar using 2-propanol. This mixture was initially heated at 1000°C for 24 h followed by subsequently heating at higher temperatures with intermediate grindings, until a monophasic powder was obtained. A Siefert 3000 X-ray diffractometer was used to analyze the phase purity of the sample. The powder were pressed into cylindrical pellets and heated for 16 h at 1500°C for Pr- and Nd-doped compositions and 1400°C for the Gd- and Y-doped compositions. Composition analysis was carried out using Energy Dispersive X-rays Analysis (EDAX) using a LEICA S440I scanning electron microscope fitted with an Si–Li detector. Redox titrations showed that the $Mn^{4+}$ content was close to 50% in the samples. Magnetization measurements were carried out with a vibrating sample magnetometer (Lakeshore VSM 7300) in the temperature range 50–300 K equipped with a closed cycle helium cryostat. The applied field was fixed at 200 Oe. Electrical resistivity measurements were made in the standard four-point configuration in the temperature range 30–300 K.

## 3. Results and discussion

In $La_{0.5-x}Pr_xSr_{0.5}MnO_3$, we observe a definitive change in the crystal structure around $x = 0.2$, from the $I4/mcm$ structure to one of lower symmetry as seen from the XRD patterns in Fig. 1. The unit cell parameters show a crossover at this composition (Fig. 2). We have preferred to assign an orthorhombic

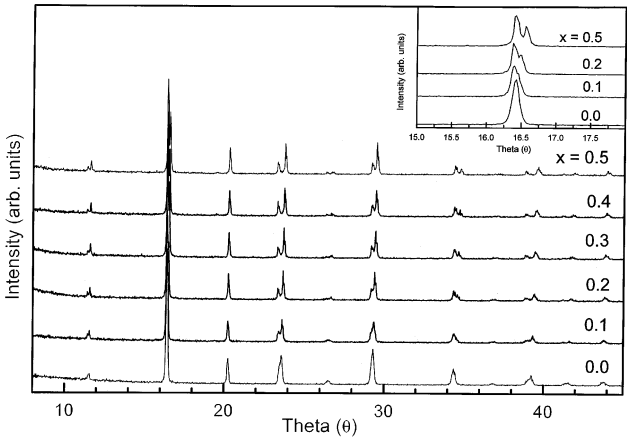


Fig. 1. Powder diffraction pattern of $La_{0.5-x}Pr_xSr_{0.5}MnO_3$ at different substitution levels. Inset shows the expanded region of theta value between 15° and 18° to show the structural transformation.

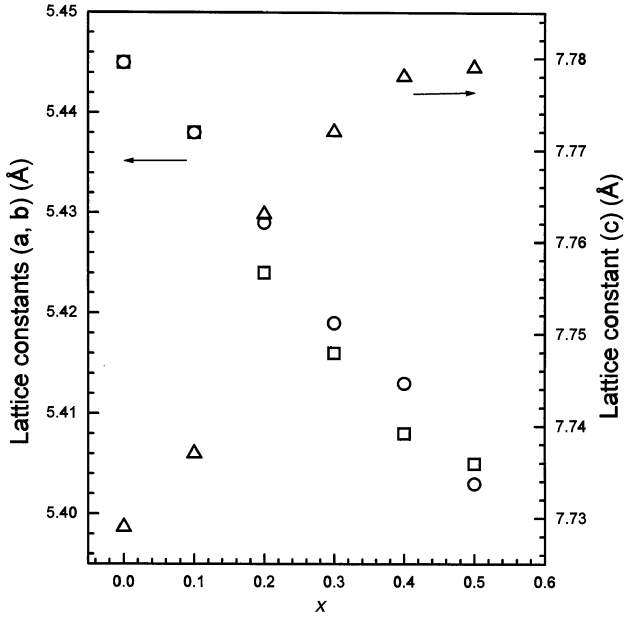


Fig. 2. The variation of lattice parameters with $x$ of $La_{0.5-x}Pr_xSr_{0.5}MnO_3$.

Table 1
Lattice parameters of $La_{0.5-x}Ln_xSr_{0.5}MnO_3$ ($Ln$ = Pr and Nd)

| $x$ | S.G. | Lattice parameters | | | | | |
|---|---|---|---|---|---|---|---|
| | | $\langle r_A \rangle$ (Å) | $\sigma^2$ (Å$^2$) | $a$ (Å) | $b$ (Å) | $c$ (Å) | $V$ (Å$^3$) |
| $Ln$ = Pr | | | | | | | |
| 0 | $I4/mcm$ | 1.263 | 0.0022 | 5.445 | 5.445 | 7.729 | 229.149 |
| 0.1 | $I4/mcm$ | 1.259 | 0.0027 | 5.438 | 5.438 | 7.737 | 228.797 |
| 0.2 | $Immm$ | 1.256 | 0.0031 | 5.424 | 5.429 | 7.763 | 228.596 |
| 0.3 | $Immm$ | 1.252 | 0.0035 | 5.416 | 5.419 | 7.772 | 228.103 |
| 0.4 | $Immm$ | 1.248 | 0.0039 | 5.408 | 5.413 | 7.778 | 227.689 |
| 0.5 | $Immm$ | 1.245 | 0.0043 | 5.405 | 5.403 | 7.779 | 227.172 |
| $Ln$ = Nd | | | | | | | |
| 0 | $I4/mcm$ | 1.263 | 0.0022 | 5.445 | 5.445 | 7.729 | 229.149 |
| 0.1 | $I4/mcm$ | 1.258 | 0.0029 | 5.436 | 5.436 | 7.677 | 226.856 |
| 0.25 | $I4/mcm$ | 1.249 | 0.0039 | 5.423 | 5.423 | 7.667 | 225.478 |
| 0.3 | $I4/mcm$ | 1.247 | 0.0043 | 5.422 | 5.429 | 7.665 | 225.627 |
| 0.35 | $Imma$ | 1.244 | 0.0046 | 5.419 | 5.426 | 7.661 | 225.260 |
| 0.4 | $Imma$ | 1.242 | 0.0049 | 5.417 | 5.424 | 7.659 | 225.035 |
| 0.5 | $Imma$ | 1.236 | 0.0054 | 5.413 | 5.420 | 7.653 | 224.486 |

*Immm* structure to the $x \geqslant 0.2$ compositions since it gave the best fit to the experimental data. The $x = 0.5$ composition ($Pr_{0.5}Sr_{0.5}MnO_3$) has been assigned different space groups including orthorhombic *Pbnm* or *Imma*, tetragonal $F4/mmc$ or $I4/mcm$ [2,22]. The unit cell volume of $La_{0.5-x}Pr_xSr_{0.5}MnO_3$ decreases with increase in $x$ or decrease in $\langle r_A \rangle$ as expected (Table 1). In Fig. 3(a), we show the magnetization data of the $La_{0.5-x}Pr_xSr_{0.5}MnO_3$ compositions. The $x = 0.0$ composition is ferromagnetic (FM) with a $T_C$ well above room temperature ($\sim$350 K), as reported in the literature [2]. With increase in $x$, the ferromagnetic $T_C$ decreases, the value being around 325, 315, 300, 278 K, respectively for the $x = 0.1$, 0.2, 0.3 and 0.4 compositions. Distinct AFM transitions are seen when $x > 0.2$, with $T_N$ values of 100 and 123 K for the $x = 0.3$ and 0.4 compositions, respectively. The $T_N$ value for the $x = 0.2$ composition is well below 80 K. Thus, the $T_C - T_N$ gap decreases with increase in $x$, being 110 K when $x = 0.5$ and 200 K when $x = 0.3$. We notice that the $\sigma^2$ also increases with increase in $x$.

Electrical resistivity data of $La_{0.5-x}Pr_xSr_{0.5}MnO_3$ are presented in Fig. 3(b). The $x = 0.0$ composition is metallic, while the $x = 0.5$ composition shows an increase in resistivity at $T_N$ (150 K), although the increase is not as pronounced as in $Nd_{0.5}Sr_{0.5}MnO_3$ where charge ordering occurs [3,4]. The $x = 0.3$ and 0.4 compositions show a small similar increase in resistivity around $T_N$ and the change is negligible in the $x = 0.1$ and 0.2 compositions.

In Fig. 4, we show the powder X-ray diffraction patterns of $La_{0.5-x}Nd_xSr_{0.5}MnO_3$ and list the lattice parameters in Table 1. The data reveal a transition from the $I4/mcm$ structure to the *Imma* structure [23] around a composition of $x = 0.35$ (Fig. 4). There is a progressive decrease in the unit cell volume with increase

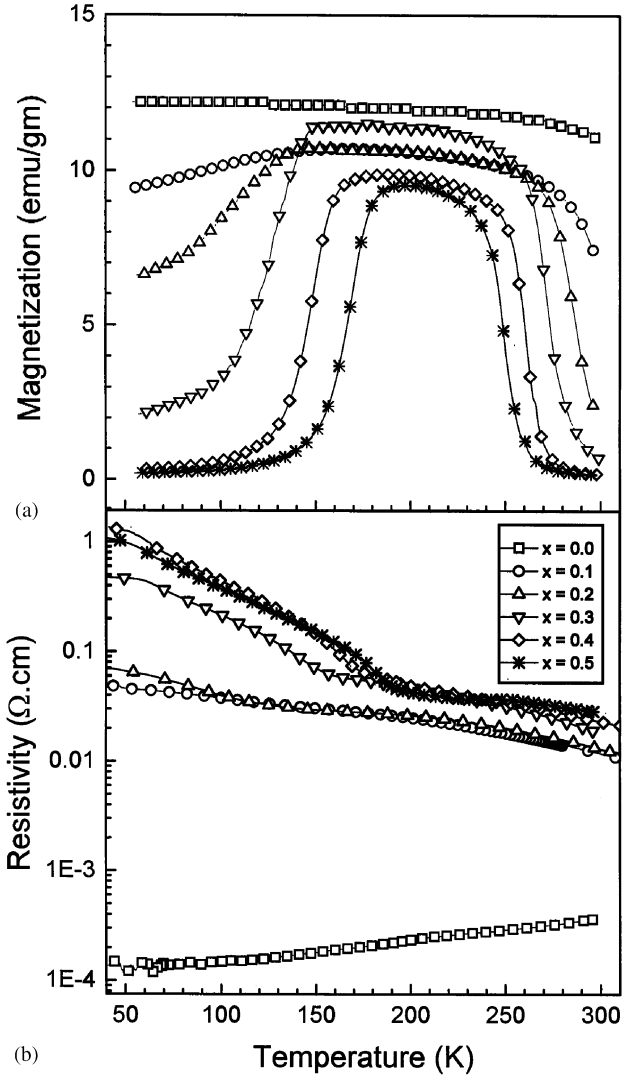


Fig. 3. The variation of (a) magnetization, and (b) resistivity as a function of temperature of $La_{0.5-x}Pr_xSr_{0.5}MnO_3$.

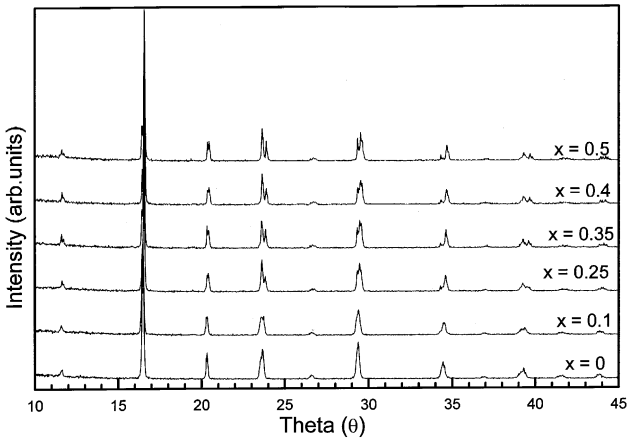


Fig. 4. Powder diffraction pattern of $La_{0.5-x}Nd_xSr_{0.5}MnO_3$ at different substitution levels.

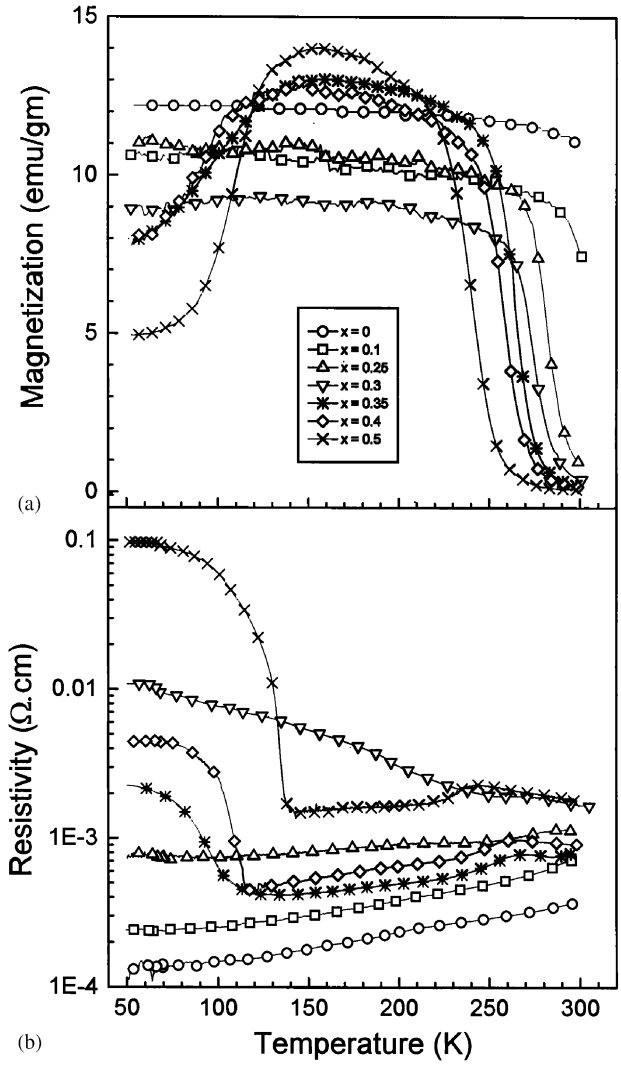


Fig. 5. Temperature-dependence behavior of (a) magnetization, and (b) resistivity of $La_{0.5-x}Nd_xSr_{0.5}MnO_3$.

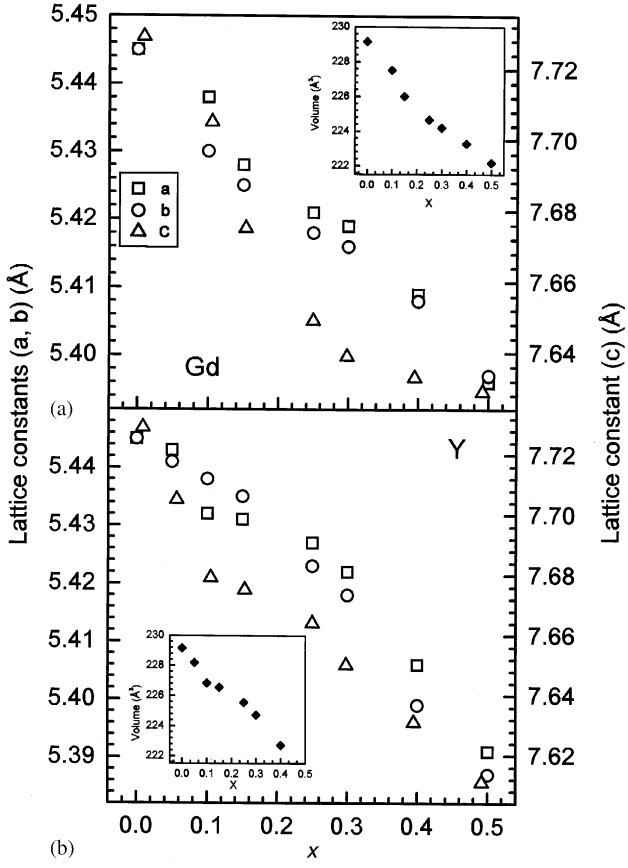


Fig. 6. The variation of lattice parameters with $x$ of (a) $La_{0.5-x}Gd_xSr_{0.5}MnO_3$, and (b) $La_{0.5-x}Y_xSr_{0.5}MnO_3$. The insets show corresponding unit cell volume.

in $x$ as expected (Table 1). In Fig. 5(a), we show the magnetization data of $La_{0.5-x}Nd_xSr_{0.5}MnO_3$. With increase in $x$, the ferromagnetic $T_C$ decreases just as in $La_{0.5-x}Pr_xSr_{0.5}MnO_3$, the $T_C$ values of the $x = 0.1$, 0.25 and 0.3 compositions being around 325, 293 and 283 K, respectively, but do not exhibit antiferromagnetism at low temperatures. The $x = 0.35$ and 0.4 compositions become ferromagnetic around 272 and 260 K, respectively, followed by a sharp decrease in magnetization around 135 K, a behavior similar to that of $Nd_{0.5}Sr_{0.5}MnO_3$ ($x = 0.5$). The sharp drop in magnetization in the $x \geqslant 0.35$ compositions is clearly due to the occurrence of an antiferromagnetic (AFM) transition.

Electrical resistivity data of $La_{0.5-x}Nd_xSr_{0.5}MnO_3$ are shown in Fig. 5(b). The compositions up to $x = 0.25$ are metallic below room temperature. The $x \geqslant 0.35$ compositions show a transition to a metallic state around 250 K followed by a sharp transition to an insulating state in the 120–150 K region. These two transitions are clearly linked to the onset of the FM and AFM states, just as in $Nd_{0.5}Sr_{0.5}MnO_3$.

The $La_{0.5-x}Ln_xSr_{0.5}MnO_3$ ($Ln$ = Gd and Y) compositions are all orthorhombic (*Pbnm*) and show a decrease in the lattice parameters and unit cell volumes with an increase in $x$ as shown in Fig. 6. In Fig. 7(a), we show the magnetization data of $La_{0.5-x}Gd_xSr_{0.5}MnO_3$. The ferromagnetic $T_C$ decreases with the increase in $x$ up to 0.15. Although the magnetization data reveal a ferromagnetic $T_C$ for $x = 0.1$, the resistivity data in Fig. 7(b) do not show a clear metallic behavior below $T_C$. The composition with $x = 0.15$ shows the FM and AFM transitions with $T_C$ and $T_N$ values of $\sim$250 and $\sim$170 K, respectively. The $x = 0.15$ composition does not show a sharp resistivity transition at $T_N$ just as $La_{0.5-x}Pr_xSr_{0.5}MnO_3$ (see Fig. 3(b)). In the $0.15 < x < 0.4$ compositions, we do not observe a sharp $T_C$, but instead see broad peaks in the magnetization data. This behavior suggests a competition between FM and AFM interactions in these compositions not unlike that near the charge-ordering transition in some of the manganates. The $x = 0.5$ composition is known to exhibit a cluster glasslike behavior at low temperatures [6,7] and it

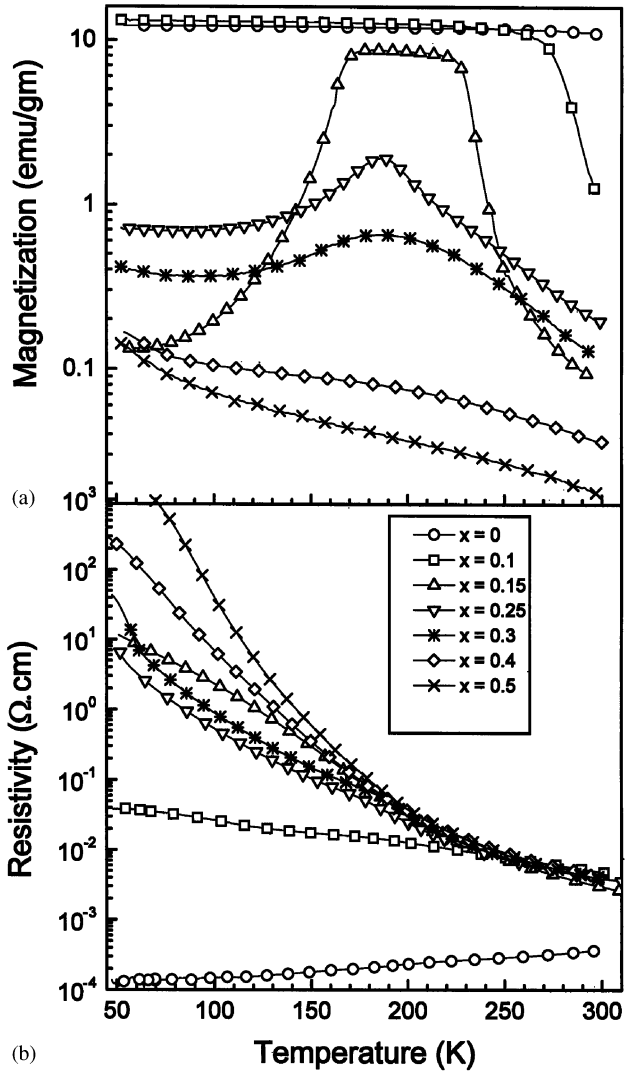


Fig. 7. The variation of (a) magnetization, and (b) resistivity as a function of temperature of $La_{0.5-x}Gd_xSr_{0.5}MnO_3$.

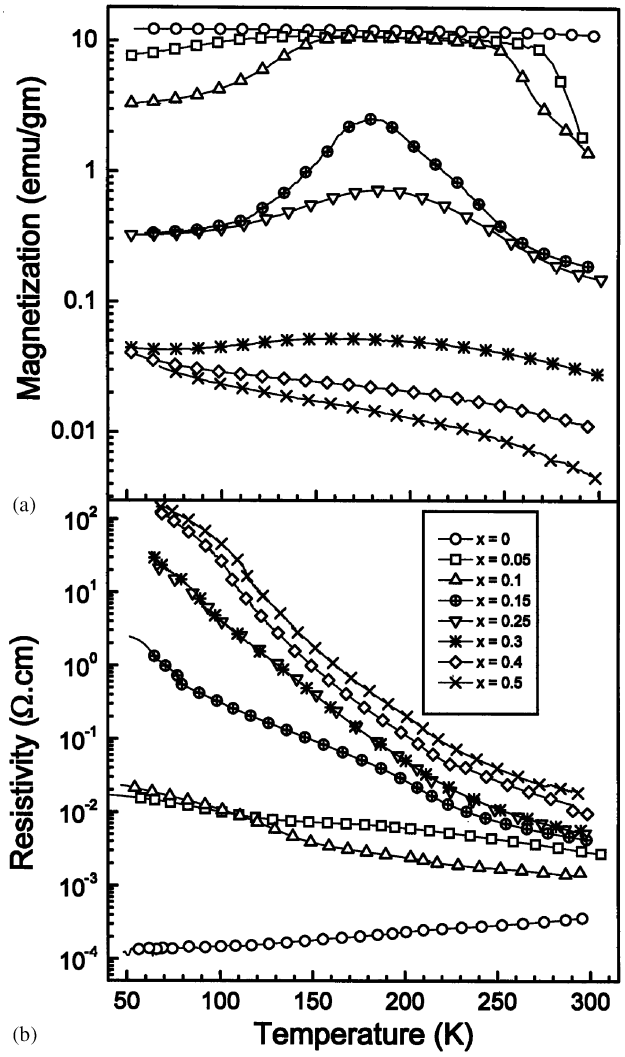


Fig. 8. The variation of (a) magnetization, and (b) resistivity as a function of temperature of $La_{0.5-x}Y_xSr_{0.5}MnO_3$.

is possible that the $x = 0.4$ composition has similar properties.

The magnetization and resistivity data of the $La_{0.5-x}Y_xSr_{0.5}MnO_3$ compositions shown in Fig. 8, reveal their properties to be similar to those of $La_{0.5-x}Gd_xSr_{0.5}MnO_3$ except that a clear ferromagnetic $T_C$ occurs only when $x \leqslant 0.1$. This is due to the much smaller size of Y compared to Gd. The $x = 0.1$ composition shows a broad AFM transition at low temperatures just as the $x = 0.15$ composition in the Gd system. There is no appreciable change in the resistivity at the AFM transition in the Y-substituted manganates as well.

We find that the plots of $T_C$ against $\langle r_A \rangle$ for the ferromagnetic $La_{0.5-x}Ln_xSr_{0.5}MnO_3$ compositions are linear as expected, the positive slope of the plot varying in the order $Pr \cong Nd < Gd < Y$. The $T_N$ data of the compositions which become antiferromagnetic at lower temperatures indicate that $T_N$ decreases with increase in $\langle r_A \rangle$.

The magnetic properties of $La_{0.5-x}Ln_xSr_{0.5}MnO_3$ ($Ln$ = Gd and Y) compositions with $\langle r_A \rangle$ close to that of $Pr_{0.5}Sr_{0.5}MnO_3$ are interesting. We show the magnetization data for four such compositions in Fig. 9. They all show a FM transition just below room temperature and an AFM transition at low temperatures. The ferromagnetic $T_C$ decreases while the $T_N$ increases as we go from composition 1 to 4. The only variable in this series is the size disorder as measured by $\sigma^2$. Surprisingly, the $\sigma^2$ increases only slightly through 1 to 4 and yet causes large changes in $T_C$ and $T_N$. We have plotted the variation of $T_C$ and $T_N$ with $\sigma^2$ in Fig. 10(a) and (b), respectively. The data show a decrease in $T_C$ with increasing $\sigma^2$, accompanied by an increase in $T_N$. Accordingly, the $T_C - T_N$ window decreases with increase in $\sigma^2$ as shown in Fig. 10(c), a feature noticed earlier in $La_{0.5-x}Pr_xSr_{0.5}MnO_3$ (Fig. 3(a)). We obtained

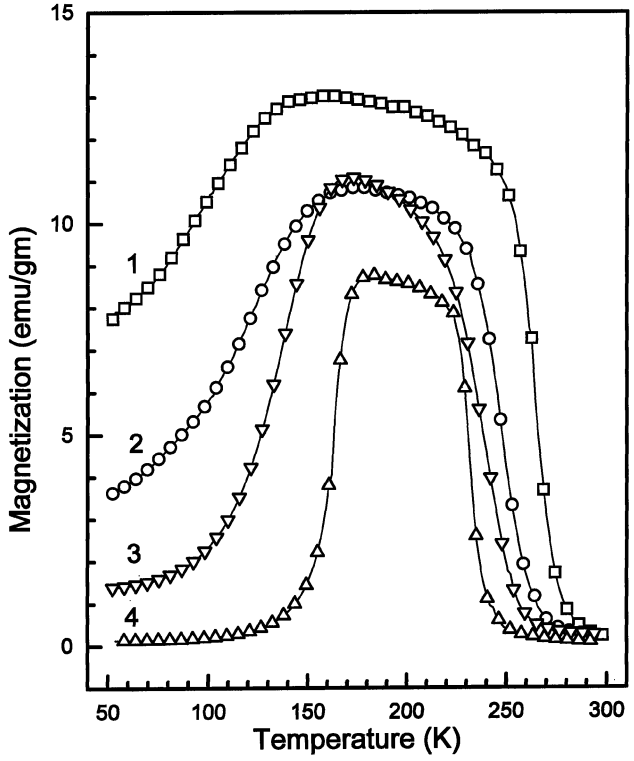


Fig. 9. Temperature-dependence behavior of magnetization of (1) $La_{0.15}Nd_{0.35}Sr_{0.5}MnO_3$, (2) $La_{0.3}Sm_{0.2}Sr_{0.5}MnO_3$, (3) $La_{0.35}Gd_{0.15}Sr_{0.5}MnO_3$, and (4) $La_{0.42}Yb_{0.08}Sr_{0.5}MnO_3$.

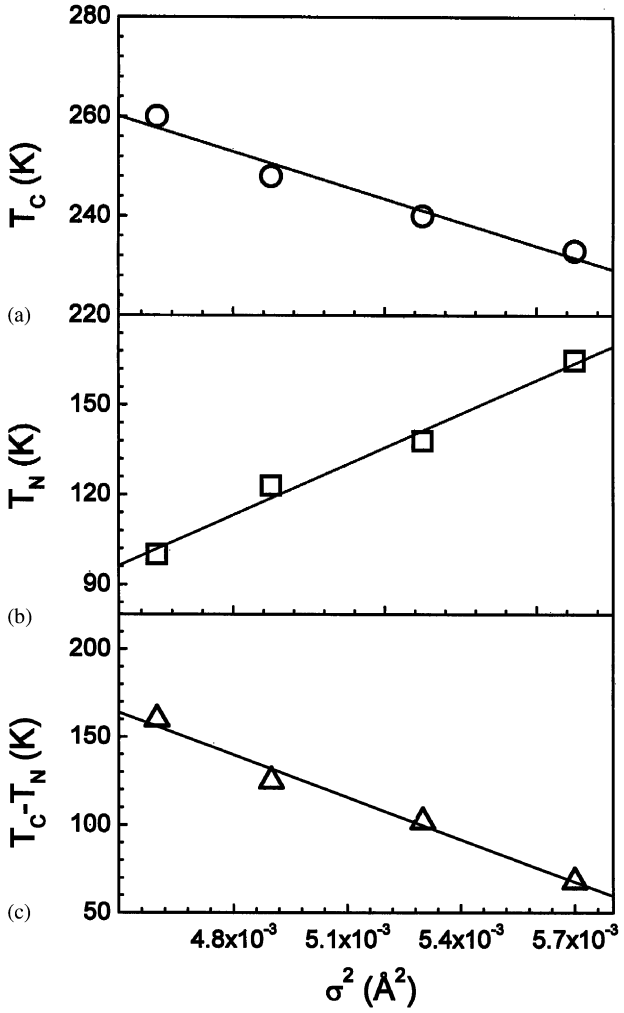


Fig. 10. Variation of (a) $T_C$, (b) $T_N$ and (c) $T_C-T_N$ with $\sigma^2$ of (1) $La_{0.15}Nd_{0.35}Sr_{0.5}MnO_3$, (2) $La_{0.3}Sm_{0.2}Sr_{0.5}MnO_3$, (3) $La_{0.35}Gd_{0.15}Sr_{0.5}MnO_3$, and (4) $La_{0.42}Yb_{0.08}Sr_{0.5}MnO_3$.

the slope of 23,000 K Å$^{-2}$ from the $\sigma^2$ versus $T_C$ plot in Fig. 10. For a similar $\langle r_A \rangle$ value, Vanitha et al. [24] have reported a slope of 15,000 K Å$^{-2}$ and an intercept $T_C^0$ of $331 \pm 13$ K. The intercept of 360 K obtained by us is comparable. The intercept found by Vanitha et al. [24] is comparable to that in $(La_{1-x}Ln_x)_{0.7}Ca_{0.3}MnO_3$ [10]. It has been suggested that the $T_C^0$ increases with increase in $\langle r_A \rangle$ [10]. The $T_C^0$ found by us is consistent with this suggestion.

In $La_{0.5-x}Ln_xSr_{0.5}MnO_3$ ($Ln$ = Pr, Nd, Gd and Y), the cation size disorder, $\sigma^2$, increases with an increase in $x$, accompanied by a decrease in $\langle r_A \rangle$. The variance in the distribution of Mn–O and $A$–O distances, $\sigma^2$ (Mn–O) and $\sigma^2$ ($A$–O), respectively, contribute to the total $\sigma^2$. The $\sigma^2$ (Mn–O) quantifies the orthorhombic distortion and $\sigma^2$ ($A$–O) quantifies the local distortion [9,13]. For a fixed Jahn–Teller distortion one would expect a major contribution to the $\sigma^2$ to come from $\sigma^2$ ($A$–O). This can provide a qualitative explanation of the different slopes of $T_C$ against $\langle r_A \rangle$ observed in the $La_{0.5-x}Ln_xSr_{0.5}MnO_3$ series. As the local distortion increases, there is increasing electron localization, and hence the decrease in $T_C$. As one goes from Pr to Y, $\sigma^2$ ($A$–O) increases parallelly with the decrease in $T_C$. The linear variation of $T_C$ with $\sigma^2$ found for a fixed $\langle r_A \rangle$ of $1.245 \pm 0.001$ Å suggests that incoherent lattice distortions may strongly influence electron transport and magnetic properties of the manganates.

Rare earth manganates of the type $Ln_{1-x}A_xMnO_3$ show evidence for electronic phase separation especially for the narrow band systems such as those with $A$ = Ca [10,25,26]. Accordingly, phase separation has been found in $La_{0.5}Ca_{0.5}MnO_3$ and $Pr_{0.7}Ca_{0.3}MnO_3$. Such phase separation is normally not found at large $\langle r_A \rangle$ values. Recent studies show that phase separation is particularly favored when $\langle r_A \rangle \leqslant 1.19$ Å [10]. It is in this regime that one finds the coexistence of phases with different electronic and magnetic properties. In the manganates that we have studied here, the $\langle r_A \rangle$ is above the 1.23 Å and we have not found obvious effects due to electronic phase separation in the measurements carried out by us. Careful measurements at low temperatures may, however, reveal phase separation in some of them.

## 4. Conclusions

Magnetic and electron transport properties of manganates of the type $La_{0.5-x}Ln_xSr_{0.5}MnO_3$ ($Ln$ = Pr, Nd, Gd and Y), with a fixed carrier concentration, vary markedly with the rare earth as well as composition. Both $Ln$ and $x$ affect $\langle r_A \rangle$, which in turn affects the local structure and the properties. Thus, as La is progressively replaced by a smaller rare earth ion, the ferromagnetic $T_C$ decreases and the material becomes antiferromagnetic at lower temperatures, the type of antiferromagnetic ordering depending on the rare earth ion. Local structural changes due to the A-site cation size mismatch also play a role in determining the transport and magnetic properties of the mangantes. Interestingly, the $T_C - T_N$ gap in the manganates decreases significantly with the increase in the size mismatch.

## Acknowledgments

The authors thank BRNS (DAE, India) for support of this research. One of us (MMS) thanks Council of Scientific and Industrial Research (CSIR, India) for a research fellowship.

## References

[1] C.N.R. Rao, B. Raveau, Colossal Magnetoresistance, Charge Ordering and Related properties of Manganese Oxides, World Scientific, Singapore, 1998.
[2] O. Chmaissem, B. Dabrowski, S. Kolesnik, J. Mais, J.D. Jorgensen, S. Short, Phys. Rev. B 67 (1995) 94431.
[3] H. Kuwahara, Y. Tomioka, A. Asamitsu, Y. Tokura, Science 270 (1995) 961.
[4] C.N.R. Rao, J. Phys. Chem. B 104 (2000) 5877.
[5] C.N.R. Rao, A. Arulraj, A.K. Cheetham, B. Raveau, J. Phys.: Condens. Matter 12 (2000) R83.
[6] A. Maignan, C. Martin, F. Damay, B. Raveau, Chem. Mater. 10 (1998) 950.
[7] T. Terai, T. Sasaki, T. Kakeshita, T. Fukuda, T. Saburi, H. Kitagawa, K. Kindo, M. Honda, Phys. Rev. B 61 (2000) 3488.
[8] L.M. Rodriguez-Martinez, J.P. Attfield, Phys. Rev. B 54 (1996) R15622.
[9] L.M. Rodriguez-Martinez, J.P. Attfield, Chem. Mater. 11 (1999) 1504.
[10] L. Sudheendra, C.N.R. Rao, J. Phys.: Condens. Matter 15 (2003) 3029.
[11] R. Mahesh, R. Mahendiran, A.K. Raychaudhuri, C.N.R. Rao, J. Solid State Chem. 120 (1995) 204.
[12] P.G. Radaelli, D.E. Cox, M. Marezio, S.-W. Cheong, Phys. Rev. B 55 (1997) 3015.
[13] P.G. Radaelli, G. Iannone, M. Marezio, H.Y. Hwang, S-W. Cheong, J.D. Jorgensen, D.N. Argyriou, Phys. Rev. B 56 (1997) 8265.
[14] A. Arulraj, P.N. Santosh, A. Guha, A.K. Raychaudhuri, N. Kumar, C.N.R. Rao, J. Phys.: Condens. Matter 10 (1998) 8497.
[15] S. Chatterjee, A.K. Nigam, Phys. Rev. B 66 (2002) 104403.
[16] D. Louca, T. Egami, E.L. Brosha, H. Röder, A.R. Bishop, Phys. Rev. B 56 (1997) R8475.
[17] H. Kawano, R. Kajimoto, H. Yoshizawa, Y. Tomioka, H. Kuwahara, Y. Tokura, Phys. Rev. Lett. 78 (1997) 4253.
[18] F. Damay, C. Martin, M. Hervieu, A. Maignan, B. Raveau, G. Andre, F. Bouree, J. Magn. Magn. Mater. 184 (1998) 71.
[19] J. Fontcuberta, V. Laukhin, X. Obradors, Phys. Rev. B 60 (1999) 6266.
[20] C. Martin, A. Maignan, M. Hervieu, B. Raveau, Phys. Rev. B 60 (1999) 12191.
[21] K.V. Sarathy, N. Utkarsh, C.N.R. Rao, Mater. Res. Bull. 37 (2002) 1785.
[22] P.M. Woodward, T. Vogt, D.E. Cox, A. Arulraj, C.N.R. Rao, P. Karen, A.K. Cheetham, Chem. Mater. 10 (1998) 3652.
[23] P.M. Woodward, T. Vogt, D.E. Cox, A.K. Cheetham, C.N.R. Rao, Chem. Mater. 11 (1999) 3528.
[24] P.V. Vanitha, P.N. Santhosh, R.S. Singh, C.N.R. Rao, J.P. Attfield, Phys. Rev. B 59 (1999) 13539.
[25] P.V. Vanitha, C.N.R. Rao, J. Phys.: Condens. Matter 13 (2001) 11707.
[26] E. Dagotto, Nanoscale Phase Separation and Colossal Magnetoresistance the physics of manganites and related compounds, Springer-Verlag, Berlin, New York, 2003.